Metabolic Engineering 10 (2008) 227–233

Contents lists available at ScienceDirect

Metabolic Engineering

journal homepage: www.elsevier.com/locate/ymben

Selection of objective function in genome scale flux balance analysis for process feed development in antibiotic production

Chiraphan Khannapho [1], Hongjuan Zhao, Bhushan K. Bonde, Andrzej M. Kierzek, Claudio A. Avignone-Rossa, Michael E. Bushell *

Microbial Science Division, Faculty of Health and Medical Sciences, University of Surrey, Guildford, Surrey GU2 7XH, UK

ARTICLE INFO

Article history:
Received 5 October 2007
Received in revised form
12 February 2008
Accepted 9 June 2008
Available online 17 June 2008

Keywords:
Process feed design
Metabolic flux variability analysis
Streptomyces coelicolor
Genome scale

ABSTRACT

Using flux variability analysis of a genome scale metabolic network of *Streptomyces coelicolor*, a series of reactions were identified, from disparate pathways that could be combined into an actinorhodin-generating mini-network. Candidate process feed nutrients that might be expected to influence this network were used in process simulations and *in silico* predictions compared to experimental findings. Ranking potential process feeds by flux balance analysis optimisation, using either growth or antibiotic production as objective function, did not correlate with experimental actinorhodin yields in fed processes. However, the effect of the feeds on glucose assimilation rate (using glucose uptake as objective function) ranked them in the same order as *in vivo* antibiotic production efficiency, consistent with results of a robustness analysis of the effect of glucose assimilation on actinorhodin production.

1. Introduction

Genome scale metabolic network modelling has been used for pragmatic process design for antibiotic production in *Streptomyces coelicolor* cultures (Bushell et al., 2006a, b). This study investigated the use of flux balance analysis (FBA) based computational approaches. FBA modelling makes the assumption that metabolic network fluxes will reach a steady state, constrained by the stoichiometry of the network (Kauffman et al., 2003). Despite this method resulting in an initially underdetermined system, a bounded solution space, containing all feasible fluxes within the network can be computed (Schilling et al., 2000). The solution space can be reduced further by specifying maximum and minimum fluxes through any particular reaction and then further refined by adding experimental data or examining responses to the imposition of hypothetical reaction fluxes (Schilling et al., 2000). The publication of the *S. coelicolor* genome sequence (Bentley et al., 2002) has allowed the construction of a genome scale metabolic network for the species providing the framework for FBA simulation of a *Streptomyces* species (Borodina et al., 2005). Maximisation of cell growth or biomass biosynthesis rate is commonly employed as the objective function of FBA simulations (Edwards et al., 2001; Edwards and Palsson, 2000; Forster et al., 2003; Ibarra et al., 2002; Reed et al., 2003; Schilling et al., 2002; Varma and Palsson, 1993, 1994). However, numerous other potentially useful objective functions exist, and it is now possible to compare them systematically in order to select the most appropriate one (Patil et al., 2005; Knorr et al., 2007). Simulation of antibiotic production presents a novel challenge in defining the objective function since antibiotics are secondary metabolites and are not required for cell growth. Furthermore, under many circumstances, optimal cell growth and optimal secondary metabolism may be thought of as being mutually exclusive (Bibb, 2005) as reduction in growth rate commonly induces secondary metabolism irrespective of the nutrient status of the culture (Bushell et al., 1997).

Metabolic flux analysis differs from FBA in that optimisation algorithms are not employed, the approach relying on experimentally determined flux estimates to reduce the underdetermined nature of the network (Stephanopoulos et al., 1998). This has been applied successfully to process design, using small metabolic networks, to a number of bioproducts including production of recombinant DNA for gene therapy (Rozkov et al., 2004) and antibiotic yield optimisation (Bushell et al., 2006a, b). In the latter, amino acid culture feeds were devised on the basis of hypotheses, generated by simulations involving a 57 reaction network, representing *Streptomyces* metabolism. This approach also accounted for observed differential antibiotic production, depending on the identity of the growth limiting nutrient (Kirk et al., 2000). A genome scale network has been used to investigate

* Corresponding author. Fax: +441483686401.
E-mail address: m.bushell@surrey.ac.uk (M.E. Bushell).
[1] Present address: National Institute for Genetic Engineering and Biotechnology, 113 Thailand Science Park Paholyothin Road, Klong 1, Klong Luang Pathumthani 12120, Thailand.

1096-7176/$ - see front matter © 2008 Elsevier Inc. All rights reserved.
doi:10.1016/j.ymben.2008.06.003

enhanced actinorhodin production following *zwf* mutation of *S. coelicolor* (Bushell et al., 2006a, b).

2. Materials and methods

2.1. Strains and culture media

S. coelicolor strain M510 (Kieser et al., 2000), a derivative of M145, the prototrophic strain used as the source of DNA for the sequencing of the genome of *S. coelicolor* A3(2) (Bentley et al., 2002) was used throughout. M510 differs from M145 only in the deletion of *redD*, the pathway-specific activator of genes for the biosynthesis of the red pigment undecylprodigiosin. M510 was engineered to overproduce the enzymes of actinorhodin biosynthesis by the introduction of a constitutively expressed copy of *act*II-*orf*4, the pathway-specific activator of the actinorhodin pathway genes, on the integrating plasmid pIJ8714. The key features of pIJ8714 are: it is based on pSET152 (Kieser et al., 2000; Bierman et al., 1992), a plasmid that can replicate in *E. coli*, be transferred by conjugation into *S. coelicolor*, and integrate efficiently and stably into the *S. coelicolor* chromosome at the φC31 prophage attachment site; and it contains a copy of *act*II-*orf*4 under the control of the strong constitutive promoter *ermEp** (Kieser et al., 2000).

The chemically defined (phosphate limited) bioreactor medium contained the following major nutrients (mM in reverse osmosis purified water): glucose, 194; citric acid, 2; $(NH_4)_2SO_4$, 50; Na_2HPO_4, 4 (three for chemostat cultures); KCl, 10; $MgCl_2$, 1.25; Na_2SO_4, 2; $CaCl_2$, 0.25 and 5 ml l^{-1} of the following trace components (mM): ZnO, 50; $FeCl_3$, 20; $MnCl_2$, 10; $CuCl_2$, 10; $CoCl_2$, 20; H_3BO_3, 10; Na_2MoO_4, 0.02. pH was adjusted to 7.0 with HCl prior to filter sterilisation using a 0.2 μm filter (Sartorius).

S. coelicolor A3(2) strains were maintained on soy flour mannitol agar (gl^{-1}: soya flour, 20; mannitol, 20; agar, 16). Liquid cultures were prepared as follows. Spores stored in glycerol solution (50% *v/v*) in cryotubes at −80 °C were used to inoculate 250 ml Erlenmeyer flasks containing 50 ml GG1 medium (Kieser et al., 2000), which were incubated at 30 °C using triangular cross-section magnetic stirrer bars for agitation. After 48 h, 5 ml was removed from GG1 culture and used to inoculate 45 ml GYB medium (Kieser et al., 2000) following the same incubation procedure (stirred 250 ml flasks) but for 24 h. After this, 20 ml GYB culture was used to inoculate sufficient 50 ml flasks of the P-limited defined medium, described above, to provide a 24 h inoculum culture at 10% (*v/v*) for bioreactor experiments.

2.2. Bioreactor culture

An Adaptive Biosystems discovery bioreactor with a maximum working volume of 5 l was used. Agitation was provided by two disc turbine impellors rotating at 1000 rpm. Dissolved oxygen concentration in the bioreactor was monitored using a galvanic dissolved oxygen electrode (Uniprobe), and controlled by automatically varying the flow rate of sterile air through a sparger. The temperature was controlled at 30 °C. The pH was controlled to 6.80 by automatic addition of 1 M NaOH. Foaming was eliminated by including 0.001% Breox FMT30 antifoam (Water Management and Gamlen) in the culture medium.

Chemostat cultures were maintained at constant volume (1 l) with a weir overflow. The cultures were phosphate-limited and all other nutrients remained in excess throughout.

2.3. Culture supernatant analysis

Glucose was determined using an enzymatic kit (VWR International: 258264W). Ammonium was determined using a colorimetric assay kit (VWR International: 1.10024.0001). Phosphate was determined using a colorimetric assay kit (VWR International: 1.10428.0001). Nutrient concentrations were measured using an RQ-reflectoquant analyser (Merck/VWR International). Actinorhodin measurements were carried out using the method described by Bystrykh et al. (1996). Extracellular actinorhodin (i.e. in the supernatant) was analysed by placing 500 μl supernatant into a centrifuge tube to which a further 500 μl 3 M KOH was added. This was then vortexed and the absorbance measured at 640 nm using a Pharmacia Biotech Ultraspec 2000. If necessary, samples were diluted ensuring the same ratio of KOH to the supernatant was used. In the cultures where actinorhodin accumulated intracellularly, the pellet resulting from 20 ml sample was resuspended in 5 ml 3 M KOH. This suspension was sonicated (Heat Systems), on ice, for a total of 7 min (30 s on/off cycles). A further 15 ml 3 M KOH was then added and centrifuged. The process was repeated until no or negligible amounts of actinorhodin remained in the pellet. The absorbance of the supernatant was measured at 640 nm. The concentration of actinorhodin was calculated using a molar extinction coefficient (E_{640}) value of 25,320 $M^{-1}\,cm^{-1}$ (Bystrykh et al., 1996).

2.4. Flux balance analysis

The genome scale model of *S. coelicolor* metabolism (Borodina et al., 2005) was used for all metabolic simulations. These employed the FBA approach (Varma and Palsson, 1994; Schilling et al., 1999). The computational approaches employed the charge-balanced genome-scale modelling environment SimPheny (Genomatica, San Diego, California).

2.5. Metabolite/reaction connectivity analysis

To obtain the connectivity score for each metabolite and reaction with respect to 'actinorhodin', a recursive algorithm written in Python (www.python.org) was used. The genome scale model of *S. coelicolor* was converted to ScrumPy (Poolman, 2006) model format and interrogated with various graph–theoretic analysis tools (ScrumPy package PyDamage (Bonde, 2006)) (Fig. 1).

For obtaining reaction connectivity scores, reactions with involvement of 'actinorhodin' were referred as score of 1 ('seed' reactions) and reactions which are connected to these seed reactions by any metabolites were assigned the score of 2. This process was iterated over all the reactions in the network to obtain the connectivity score. Thus the integer score obtained, for each reaction, refers to the number of additional reactions needed to connect that reaction to the final actinorhodin-generating reaction. Note that this analysis was carried out on the genome-scale model, which contains significantly more possible connections than the mini-network (Fig. 2).

3. Results and discussion

3.1. Antibiotic production pattern in chemostat culture and choice of case study conditions

Chemostat culture revealed a decreasing antibiotic yield as the growth (dilution) rate was raised consistent with patterns observed with production of other secondary metabolites

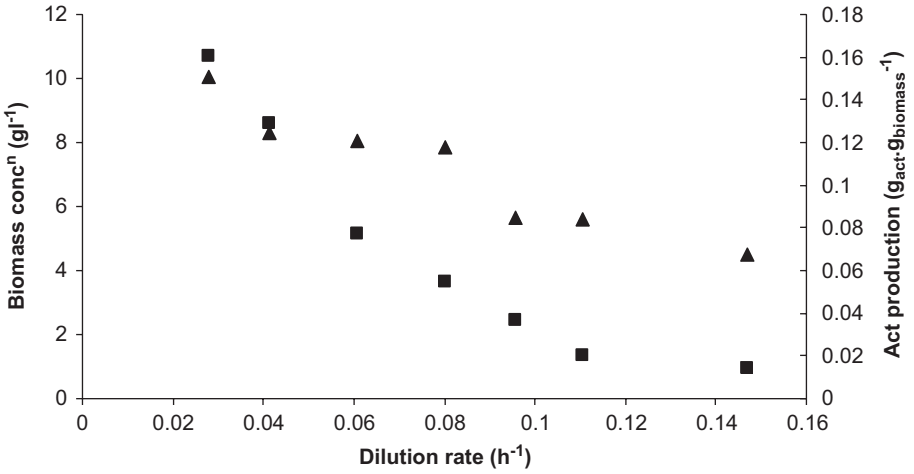

Fig. 1. Experimentally determined actinorhodin (squares) and biomass (circles) production patterns in chemostat culture.

(McDermott et al., 1993). A dilution rate of 0.04 h^{-1} was chosen for experimental feed evaluation and simulation studies, since it represented a compromise between time taken to complete each experiment and flux to antibiotic biosynthesis.

3.2. Effect of actinorhodin yield on FVA span

In a previous report (Bushell et al., 2006b), we discussed the application of FBA to pragmatic process design for antibiotic production. We used flux variability analysis (FVA) to highlight reactions whose fluxes appeared to be critical to antibiotic biosynthesis by examining the response of flux span (the difference between upper and lower flux values, capable of achieving maximum antibiotic biosynthesis rates) to antibiotic yield. This approach was adopted to address a problem with FBA, as an approach to examining flux distribution that the intermediary fluxes, computed whilst optimising the objective function are not necessarily unique and, in most cases, a range of flux values for a particular reaction can result in the same objective function value. In FVA, the objective function is set to its optimal value and then the flux through each of the 700 reactions in the network is maximised and minimised.

In our previous study (Bushell et al., 1997), we constrained a GSMN FVA simulation using experimental results and hypothesised that a decrease in FVA span, in response to mutation or process change, leading to increased antibiotic production, was indicative of the importance of the reaction in achieving the target objective function value, in response to the change. Linking the critical reactions, thus identified, that were involved in antibiotic precursor supply, resulted in an antibiotic generating mini-network, composed of reactions from numerous diverse pathways. By modelling the effect of actinorhodin biosynthesis, on the SimPheny network, comparing actinorhodin producing and non-producing FVA simulations, a list of reactions whose FVA span decreased significantly when observed rates of actinorhodin synthesis were simulated, was obtained (Table 1).

These reactions were ranked according to the effect on FVA span and those reactions connected to actinorhodin precursor biosynthesis were linked to form an actinorhodin-generating mini-network (Fig. 2).

Connectivity analyses of each metabolite to other metabolites in the whole network were computed and malcoa, the precursor for the linear actinorhodin-synthesising pathway in the genome scale network, returned a relatively low score of 4. However, the network actinorhodin-generating network obtained was more comprehensive than that reported previously (Bushell et al., 1997) and included reactions from a diverse range of metabolic pathways.

One potential drawback of this FVA-based hypothesis building is that the simulation was constrained using discrete values for actinorhodin secretion and the flux span for the secretion reaction will, therefore, be zero. Consequently, network reactions with close connectivity to the secretion reaction will also be equal to or approach zero. Thus, it was not possible to include reactions between malcoa synthesis and actinorhodin secretion in the mini-network.

Bounds for inclusion of reactions in the mini-network were set so that reactions below the first malcoa generating reaction in the ranking were excluded. Reactions not connected to act biosynthetic precursors in the mini-network (such as the futile cycle involving rnam, thmmp etc), transport reactions and ATP/ADP, GTP/GDP NAD/NADH exchange reactions (involving so-called currency metabolites) were also excluded from the figure for clarity.

3.3. Selection of process feeds

As a case study for process design, four potential nutrient feeds, potentially affecting different parts of the mini-network were selected. Citrate was chosen because according to the mini-network its biosynthesis potentially competed with that of actinorhodin for accoa (Fig. 2) and it had high actinorhodin connectivity in the mini-network. Glutamate was chosen because of its high connectivity within the mini-network. Reactions of the leucine-degradation pathway contributed to many of the immediate precursor-generating elements of the mini-network. Finally, Lysine was chosen because reactions from its degradative pathway feed into the TCA cycle via the generation of acetyl Co A (part of the TCA cycle that is included in the mini-network).

Metabolic network simulations, consisting of single optimisations were carried out, simulating the effect of feeding nutrients on the attainment of maximum actinorhodin yield, as the objective function.

Ranking the results of the simulation produced the opposite order of effectiveness of the feeds to that observed (Fig. 3). The predicted antibiotic productivity was an order of magnitude lower

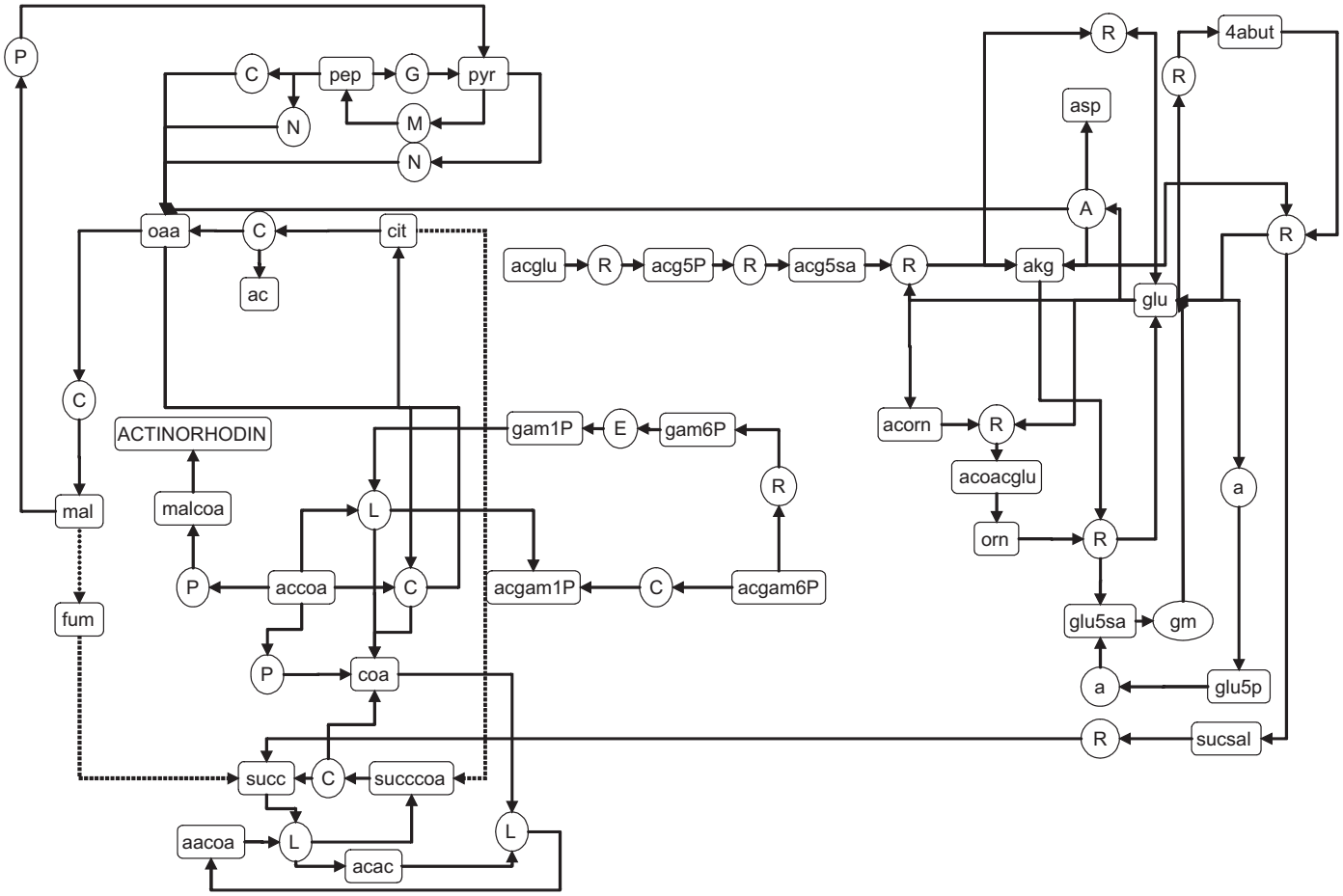

Fig. 2. Reactions with significantly reduced flux ranges in the genome scale model indicating their connectivity to each other and to actinorhodin biosynthesis. Bounds for inclusion of reactions in the mini-network were set so that reactions with lower rankings than the first malcoa generating reaction in the ranking were excluded. Reactions not connected to act biosynthetic precursors in the mini-network (such as the futile cycle involving rnam, thmmp etc), transport reactions and ATP/ADP, GTP/GDP NAD/NADH exchange reactions (involving so-called currency metabolites) were also excluded from the figure for clarity.
Reaction classes in Fig. 2:

Abbreviation	SimPheny reaction class
a	Amino acid metabolism
A	Arginine and praline metabolism
C	Citrate cycle (TCA)
E	Cell envelope biosynthesis
gm	Glutamate metabolism
G	Glycolysis
L	Leucine, isoleucine and valine biosynthesis
M	Central metabolism
N	Anaplerotic metabolism
P	Pyruvate metabolism
R	Arginine and proline metabolism.

For additional abbreviations refer Table 1 legend.

than that predicted by the simulation as the linear optimisation algorithm operates on the assumption that the network will be organised to achieve a singular objective (maximum antibiotic yield). However, in reality, cell growth is more likely to represent an objective function that represents *in vivo* network evolution (Schilling et al., 2002) particularly in the case of a secondary metabolite, which, by definition, is not required for growth.

Thus, using cell growth as the objective function results in zero antibiotic production, since, as a secondary metabolite, the biosynthesis of actinorhodin is not essential for growth and will compete with growth for biosynthetic precursor and energetic resources. The same was observed when the effect of each feed combined with varying levels of glucose uptake rate were simulated (using the "phase plane" function in SimPheny) as these too were unable to predict the effects of the feed on antibiotic production.

3.4. Effect of process feeds on glucose uptake rate and consequent antibiotic production

Single optimisation simulations (FBA optimisation using actinorhodin as the objective function and constraining the optimisation using experimentally determined feed uptake rates), were carried out to determine the effect of the process feeds on

Table 1
Reactions in the genome scale metabolic network ranked according to the decrease in FVA span when actinorhodin biosynthesis was introduced into the simulation as an additional constraint

Equation	Subsystem	Decrease in span width on Act biosynthesis	FVA_{act} F_{min}	FVA_{act} F_{max}	Actinorhodin connectivity	
					Raw	Filtered
gtp+oaa ⇔ co_2+gdp+pep	Citrate cycle (TCA)	2.80	−53.96	37.29	2	2
atp+coa+succ ⇔ adp+pi+succoa	Citrate cycle (TCA)	2.80	−53.49	33.77	2	3
mal-L+nad ⇔ h+nadh+oaa	Citrate cycle (TCA)	2.35	−50.19	26.65	2	3
accoa+pi ⇔ actp+coa	Pyruvate metabolism	1.89	−37.40	21.36	2	2
acac+succoa ⇔ aacoa+succ	Valine, leucine, and isoleucine metabolism	1.67	−49.85	3.79	3	3
adp+h+pep → atp+pyr	Glycolysis/Gluconeogenesis	1.60	0.00	53.85	2	3
acac+atp+coa → aacoa+amp+ppi	Valine, leucine, and isoleucine metabolism	1.60	0.00	49.85	2	3
mal-L+nad → co_2+nadh+pyr	Pyruvate metabolism	1.60	0.00	53.85	2	2
atp+pi+pyr → amp+h+pep+ppi	Central metabolism	1.60	0.00	49.85	2	3
accoa+h_2o+oaa → cit+coa+h	Citrate cycle (TCA)	1.35	0.00	41.08	2	2
akg+asp-L ⇔ glu-L+oaa	Alanine and aspartate metabolism	1.21	−45.56	−0.09	3	3
fdp+h_2o → f6p+pi	Glycolysis/Gluconeogenesis	1.20	0.00	37.39	2	4
glu5sa ⇔ 1pyr5c+h+h_2o	Arginine and proline metabolism	1.20	0.01	37.39	2	4
g3p+h_2o+nadp → 3pg+(2) h+nadph	Glycolysis/Gluconeogenesis	1.20	0.00	37.39	2	3
h+mmcoa-S → co_2+ppcoa	Alternate carbon metabolism	1.20	0.00	37.39	2	2
1pyr5c+(2) h_2o+nadp → glu-L+h+nadph	Arginine and proline metabolism	1.20	0.00	37.39	2	3
4abut+akg → glu-L+sucsal	Arginine and proline metabolism	1.20	0.00	37.39	3	3
acgam6p ⇔ acgam1p	Carbohydrate metabolism	1.20	−37.39	0.00	3	3
acglu+atp → acg5p+adp	Arginine and proline metabolism	1.20	0.01	37.40	2	3
ac+atp → actp+adp	Propanoate metabolism	1.20	0.00	37.40	2	3
acg5sa+glu-L → acorn+akg	Arginine and proline metabolism	1.20	0.01	37.40	3	3
actp+h_2o → ac+h+pi	Pyruvate metabolism	1.20	0.00	37.39	2	3
acgam6p+h_2o → ac+gam6p	Glutamate metabolism	1.20	0.00	37.39	2	3
acg5p+h+nadph → acg5sa+nadp+pi	Arginine and proline Metabolism	1.20	0.01	37.40	2	4
(2) ala-D+atp → adp+alaala+h+pi	Cell envelope biosynthesis	1.20	0.00	37.39	2	4
cit → ac+oaa	Citrate cycle (TCA)	1.20	0.00	37.39	3	3
accoa+gam1p → acgam1p+coa+h	Lipid and cell wall metabolism	1.20	0.01	37.40	2	2
g3p+nad+pi ⇔ 13dpg+h+nadh	Glycolysis/Gluconeogenesis	1.20	−33.20	4.18	2	3
atp+glu-L+nh4 → adp+gln-L+h+pi	Glutamate metabolism	1.20	0.00	37.39	2	3
glu-L+h → 4abut+co_2	Glutamate metabolism	1.20	0.00	37.39	2	2
glu5sa+h_2o+nad → glu-L+(2) h+nadh	Glutamate metabolism	1.20	0.00	37.39	2	3
acorn+glu-L → acglu+orn-L	Arginine and proline metabolism	1.20	0.01	37.40	3	3
1pyr5c+(2) h_2o+nad → glu-L+h+nadh	Arginine and proline metabolism	1.20	0.00	37.39	2	3
atp+co_2+h_2o+pyr → adp+(2) h+oaa+pi	Anaplerotic reactions	1.20	0.00	37.39	2	2
atp+f6p → adp+fdp+h	Central metabolism	1.20	0.00	39.50	2	4
gam1p ⇔ gam6p	Cell envelope biosynthesis	1.20	−37.40	−0.01	3	3
co_2+h_2o+pep → h+oaa+pi	Anaplerotic reactions	1.20	0.00	37.39	2	2
atp+co_2+h_2o+ppcoa → adp+(2) h+mmcoa-S+pi	Valine, leucine, and isoleucine metabolism	1.20	0.00	37.39	2	2
h_2o+nadp+sucsal → (2) h+nadph+succ	Arginine and proline metabolism	1.20	0.00	37.39	2	4
ACP+malcoa → coa+malACP	Membrane lipid metabolism	1.20	0.04	37.43	1	1
atp+h_2o+pyr → amp+(2) h+pep+pi	Histidine metabolism	1.20	0.00	37.39	2	3
glu5p+h+nadph → glu5sa+nadp+pi	Amino acid metabolism	1.20	0.00	37.39	2	4
atp+glu-L → adp+glu5p	Amino acid metabolism	1.20	0.00	37.39	2	3
akg+orn-L → glu-L+glu5sa	Arginine and proline metabolism	1.20	0.00	37.39	3	3
accoa+atp+hco3 → adp+h+malcoa+pi	Pyruvate metabolism	1.06	0.00	37.57	1	1

Experimental values for growth rate, glucose and ammonia uptake rates and CO_2 production rate were used as constraints. Reactions involving the exchange of "currency compounds" (extracellular transport, purine and pyrimidine biosynthesis, vitamin and cofactor and atp/adp/amp exchange reactions) were removed for brevity. Connectivity (raw and filtered to eliminate reactions connected by currency metabolites) was estimated as described in the text.
13dpg, 3-Phospho-D-glyceroyl phosphate; 1pyr5c, 1-Pyrroline-5-carboxylate; 3pg, 3-phospho-D-glycerate; aacoa, acetoacetyl Co A; abut, 4-aminobutanoate; ac, acetate; acac, acetoacetate; accoa, acetyl Co A; acg5p, *N*-Acetyl-L-glutamyl 5-phosphate; acg5sa, *N*-Acetyl-L-glutamate 5-semialdehyde; acgam1p, *N*-Acetyl-D-glucosamine 1-phosphate; acgam6p, *N*-Acetyl-D-glucosamine 6-phosphate; acglu, *N*-Acetyl-L-glutamate; acorn, *N*2-Acetyl-L-ornithine, act, actinorhodin; actp, acetyl phosphate; akg, alpha ketoglutarate; alaala, D-alanyl D-alanine; ala-D, D-alanine; asp-L, aspartate; cit, citrate; coa, Co A; f6p, fructose-6-phosphate; fdp, fructose-di-phosphate; g3p, Glyceraldehyde 3phosphate; gam1p, D-Glucosamine 1-phosphate; gam6p, D-Glucosamine 6-phosphate; gln, glutamine; glu, glutamate; glu5P, L-Glutamate 5-phosphate; glu5sa, L-Glutamate 5-semialdehyde; malACP, Malonyl-[acyl-carrier protein]; malcoa, malonyl Co A; mal-L, L-malate; mmcoa-S, (S)-Methylmalonyl-CoA; oaa, oxaloacetate; pep, phosphoenolpyruvate; ppcoa, Propanoyl-CoA; pyr, pyruvate; succ, succinate; succoa, succinyl Co A; sucsal, Succinic semialdehyde.

glucose uptake rate. Predicted glucose assimilation rates were ranked in the same order as the effects of the feeds on antibiotic production (Fig. 4).

The effect of varying glucose assimilation rates on antibiotic production rates was simulated using the "robustness analysis" (Edwards and Palsson, 2000) feature of SimPheny. This indicated that actinorhodin biosynthesis rate will, theoretically, increase with glucose uptake rate, when actinorhodin is the objective function (Fig. 5). Comparing the potential effects of the increased glucose uptake rates, stimulated by the feeds, we obtain a ranking in potential antibiotic production rates, similar to that obtained in practice (Fig. 6).

We conclude from this study, that application of FBA to metabolic engineering for optimisation of a secondary metabolite, whose production is growth dissociated, is not as straightforward as application to primary metabolites and that a more indirect approach, such as examination of the effect of process feeds on nutrient assimilation, must be undertaken. In our previous study, we concluded that the major influence of a *zwf* mutation on antibiotic production was a result of an indirect effect of the

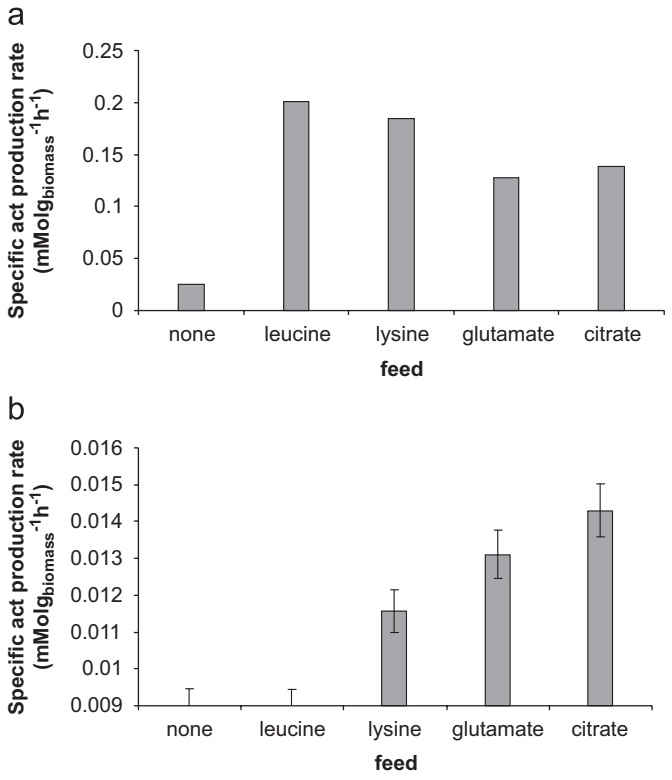

Fig. 3. (a) Predicted actinorhodin productivity with process feeds, based on robustness analysis and (b) observed actinorhodin productivity with process feeds.

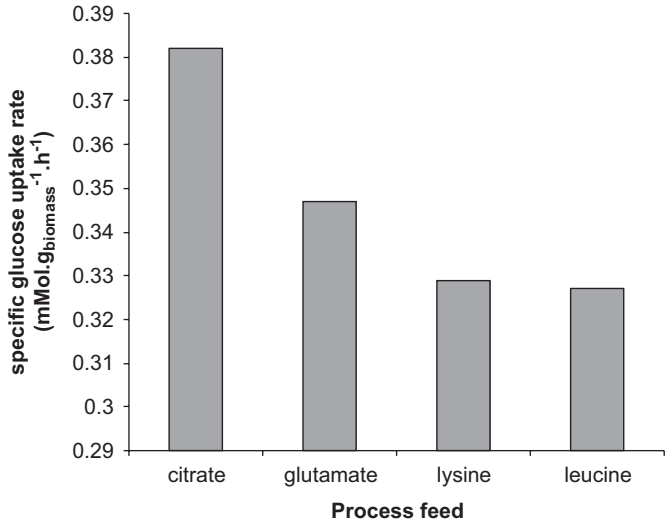

Fig. 4. Predicted effect of process feeds on glucose uptake rate obtained using single optimisation simulations.

mutation on phosphate assimilation rates. A major challenge in applying fba to secondary metabolism is determining an appropriate objective function for optimisation (Knorr et al., 2007). Growth is not appropriate since secondary metabolism is not required for it. However, antibiotic production *per se* is not appropriate since it is never the prime objective of the *in vivo* network and evolution, therefore, has not optimised the network to maximise it. Our *ad hoc* rationale for pragmatic process improvement, in this instance, was: use of FVA span response to product (objective function) induction; simulation of the effect of process feed supplement on assimilation of the primary carbon

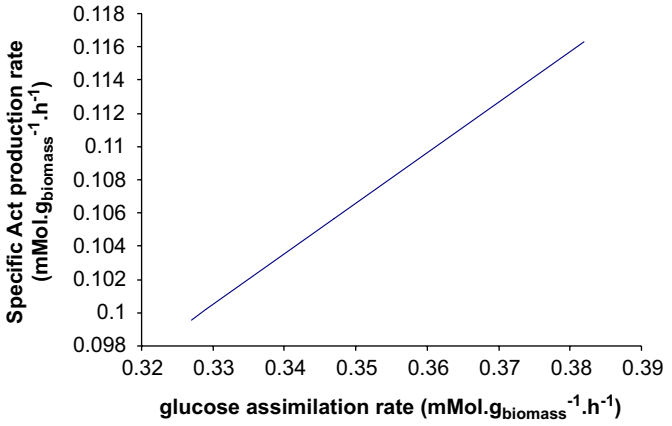

Fig. 5. Robustness analysis, simulating the effect of glucose assimilation rate on maximum antibiotic production rate.

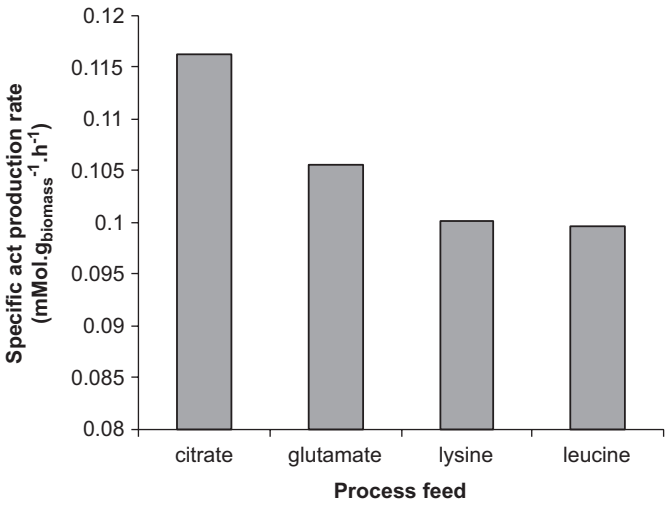

Fig. 6. Predicted effect of enhanced glucose assimilation stimulated by process feeds (at 0.05 mM.$g_{biomass}^{-1}$ h^{-1}) on Act production.

source and prediction of the effect of the resultant carbon source assimilation rate on product synthesis rate. Our findings suggest that a systematic, algorithmic approach should be developed to replace the *ad hoc* methodology employed here, possibly employing network connectivity metrics to shortlist process feed candidates. The genetic algorithmic approach of Patil et al. (2005) is an example of a rational protocol for pragmatic process design using genome scale models. An analysis of simple reaction connectivity in the genome scale network, indicated no correlation between position in the FVA ranking and connectivity (Table 1). The use of a genome scale metabolic network facilitated the introduction of reactions from a wide range of pathways into the hypothesis-generating process.

Acknowledgments

We thank BBSRC for provision of a research grant from the Engineering and Biological Systems committee.

We would like to thank Irina Borodina of Jens Nielsen's Group (Technical University of Denmark) for help and advice with implementing the genome scale metabolic network (which she developed with Prof. Nielsen (Borodina et al., 2005)), including the provision of expected values for diagnostic purposes.

References

Bentley, S.D., Chater, K.F., Cerdeno-Tarraga, A.M., Challis, G.L., Thomson, N.R., James, K.D., Harris, D.E., Quail, M.A., Kieser, H., Harper, D., Bateman, A., Brown, S., Chandra, G., Chen, C.W., Collins, M., Cronin, A., Fraser, A., Goble, A., Hidalgo, J., Hornsby, T., Howarth, S., Huang, C.H., Kieser, T., Larke, L., Murphy, L., Oliver, K., O'Neil, S., Rabbinowitsch, E., Rajandream, M.A., Rutherford, K., Rutter, S., Seeger, K., Saunders, D., Sharp, S., Squares, R., Squares, S., Taylor, K., Warren, T., Wietzorrek, A., Woodward, J., Barrell, B.G., Parkhill, J., Hopwood, D.A., 2002. Complete genome sequence of the model actinomycete *Streptomyces coelicolor* A3(2). Nature 417, 141–147.

Bibb, M.J., 2005. Regulation of secondary metabolism in streptomycetes. Curr. Opinion Microbiol. 8 (2), 208–215.

Bierman, M., Logan, R., O'Brien, K., Seno, E.T., Nagaraja Rao, R., Schoner, 1992. Plasmid cloning vectors for the conjugal transfer of DNA from *Escherichia coli* to *Streptomyces* spp. Gene 116, 43–49.

Bonde, B.K., 2006. Metabolism and Bioinformatics: The Relationship between Metabolism and Genome Structure, PhD Thesis. Oxford Brookes University, UK.

Borodina, I., Krabben, P., Nielsen, J., 2005. Genome-scale analysis of *Streptomyces coelicolor* A3(2). Genome Res. 15, 820–828.

Bushell, M.E., Smith, J., Lynch, H.C., 1997. A physiological control model for erythromycin production in batch and cyclic fed batch culture. Microbiology 143, 475–480.

Bushell, M.E., Kirk, S., Zhao, H., Avignone-Rossa, C.A., 2006a. Manipulation of the physiology of clavulanic acid biosynthesis with the aid of metabolic flux analysis. Enzyme Microb. Technol. 39, 149–157.

Bushell, M.E., Sequeira, S.I.P., Khannapho, C., Zhao, H., Chater, K.F., Butler, M.J., Kierzek, A.M., Avignone-Rossa, C.A., 2006b. The use of genome scale metabolic flux variability analysis for process feed formulation based on an investigation of the effects of the zwf mutation on antibiotic production in *Streptomyces coelicolor*. Enzyme Microb. Technol. 39, 1347–1353.

Bystrykh, L.V., Fernandez Moreno, M.A., Herrema, J.K., Malpartida, F., Hopwood, D.A., Dijkhuizen, L., 1996. Production of actinorhodin-related "blue pigments" by *Streptomyces coelicolor* A3(2). J. Bacteriol. 178, 2238–2244.

Edwards, J.S., Palsson, B.O., 2000. The *Escherichia coli* MG1655 *in silico* metabolic genotype: its definition, characteristics, and capabilities. Proc. Natl. Acad. Sci. USA 97, 5528–5533.

Edwards, J.S., Ibarra, R.U., Palsson, B.O., 2001. *In silico* predictions of *Escherichia coli* metabolic capabilities are consistent with experimental data. Nat. Biotechnol. 19, 125–130.

Forster, J., Famili, I., Fu, P., Palsson, B.O., Nielsen, J., 2003. Genome-scale reconstruction of the *Saccharomyces cerevisiae* metabolic network. Genome Res. 13, 244–253.

Ibarra, R.U., Edwards, J.S., Palsson, B.O., 2002. *Escherichia coli* K-12 undergoes adaptive evolution to achieve *in silico* predicted optimal growth. Nature 420, 186–189.

Kauffman, K.J., Prakash, P., Edwards, J.S., 2003. Advances in flux balance analysis. Curr. Opinion Biotechnol. 14, 491–496.

Kirk, S., Avignone-Rossa, C.A., Bushell, M.E., 2000. Growth limiting substrate affects antibiotic production and associated metabolic fluxes in *Streptomyces clavuligerus*. Biotechnol. Lett. 22, 1803–1809.

Kieser, T., Bibb, M.J., Buttner, M.J., Chater, K.F., Hopwood, D.A., 2000. Practical *Streptomyces* Genetics. John Innes Foundation, Norwich, UK.

Knorr, A.L., Jain, R., Srivastava, R., 2007. Bayesian-based selection of metabolic objective functions. Bioinformatics 23, 351–357.

McDermott, J.F., Lethbridge, G., Bushell, M.E., 1993. Estimation of the values of the kinetic constants and elucidation of trends in growth and erythromycin production in batch and continuous cultures of *Saccharopolyspora erythraea* using curve fitting techniques. Enzyme Microb. Technol. 15, 657–663.

Patil, K.R., Rocha, I., Förster, J., Nielsen, J., 2005. Evolutionary programming as a platform for *in silico* metabolic engineering BMC. Bioinformatics 6, 308.

Poolman, M.G., 2006. ScrumPy: Metabolic Modelling with Python. Systems Biology, IEE Proceedings, Vol. 153, pp. 375–378.

Reed, J.L., Vo, T.D., Schilling, C.H., Palsson, B.O., 2003. An expanded genome-scale model of *Escherichia coli* K-12 (iJR904 GSM/GPR). Genome Biol. 4, R54 (Art. No.).

Rozkov, A., Avignone-Rossa, C.A., Ertl, P.F., Jones, P., O'Kennedy, R.D., Smith, J.J., Dale, J.W., Bushell, M.E., 2004. Characterization of the metabolic burden on *Escherichia coli* DH1 cells imposed by the presence of a plasmid containing a gene therapy sequence. Biotechnol. Bioeng. 88, 909–915.

Schilling, C.H., Edwards, J.S., Palsson, B.O., 1999. Toward metabolic phenomics: analysis of genomic data using flux balances. Biotechnol. Prog. 15, 288–295.

Schilling, C.H., Edwards, J.S., Letscher, D., Palsson, B.O., 2000. Combining pathway analysis with flux balance analysis for the comprehensive study of metabolic systems. Biotechnol. Bioeng. 71, 286–306.

Schilling, C.H., Covert, M.W., Famili, I., Church, G.M., Edwards, J.S., Palsson, B.O., 2002. Genome-scale metabolic model of *Helicobacter pylori* 26695. J. Bacteriol. 184, 4582–4593.

Stephanopoulos, G., Aristodou, A., Nielsen, J., 1998. Metabolic Engineering. Academic Press Inc, San Diego.

Varma, A., Palsson, B.O., 1993. Metabolic capabilities of *Escherichia coli* 2. Optimal-growth patterns. J. Theor. Biol. 165, 503–522.

Varma, A., Palsson, B.O., 1994. Metabolic flux balancing—basic concepts, scientific and practical use. Biotechnology 12, 994–998.